

# A NEW TECHNIQUE FOR HETERODYNE SPECTROSCOPY: LEAST-SQUARES FREQUENCY SWITCHING (LSFS)

December 4, 2018

Carl Heiles

## ABSTRACT

We describe a new technique for heterodyne spectroscopy, which we call *Least-Squares Frequency Switching*, or *LSFS*. This technique avoids the need for a traditional reference spectrum, which—when combined with the on-source spectrum—introduces both noise and systematic artifacts such as “baseline wiggles”. In contrast, LSFS derives the spectrum directly, and in addition the instrumental gain profile. The resulting spectrum retains nearly the full theoretical sensitivity and introduces no systematic artifacts.

Here we discuss mathematical details of the technique and use numerical experiments to explore optimum observing schemas. We outline a modification suitable for computationally difficult cases as the number of spectral channels grows beyond several thousand. We illustrate the method with three real-life examples. In one of practical interest, we created a large contiguous bandwidth aligning three smaller bandwidths end-to-end; radio astronomers are often faced with the need for a larger contiguous bandwidth than is provided with the available correlator.

## 1. INTRODUCTION

In digital heterodyne spectroscopy, the measured spectrum is the product of the radio-frequency (RF) power and the intermediate-frequency (IF) gain spectra; to obtain the RF power spectrum, one must divide the on-source measured spectrum (the ON spectrum) by the IF gain spectrum. This is usually accomplished by dividing by a reference spectrum (the OFF spectrum), which is obtained by moving off in frequency or position. However, using such OFF spectra introduces additional noise because some observing time is spent off-source, and also introduces additional artifacts (“baseline wiggles”).

In particular, obtaining accurate spectral profiles for Galactic HI is difficult because of the difficulty in obtaining a good OFF spectrum. There is no place in the sky where

Galactic HI does not exist, so one cannot use an OFF position. Instead, the OFF spectrum is commonly obtained by taking an off-frequency spectrum, moving far enough in frequency so that the HI line is zero. This technique is known as “frequency switching”.

At many telescopes, frequency switching produces inaccurate OFF spectra. This occurs because the RF gain and/or the RF power have frequency structure. One contributor is reflections on the telescope structure, for example between the feed and the reflector. If their separation distance is  $D$ , then the reflected signal returns with a time delay  $\tau = \frac{2D}{c}$ . This produces a peak in the autocorrelation function of the received signal with delay  $\tau$ , which in turn produces a sinusoidal ripple in the frequency spectrum with period  $f_\tau = \frac{1}{\tau}$ . At Arecibo,  $f_\tau \sim 1.0$  MHz, equivalent to about  $200 \text{ km s}^{-1}$ , which is comparable to the velocity ranges of interest for many HI studies. Similarly, mm-wave telescopes used for molecular emission are much smaller than Arecibo and the line frequencies are much larger, and again the ripple is comparable to interesting line widths. Telescopes typically have many reflecting paths with different delays, so the received signal has a superposition of ripples with somewhat different periods. These ripples cannot be removed by frequency switching, and in fact are sometimes amplified by an unfortunate choice for the frequency-switching interval.

Here we describe a new approach. Instead of switching the local oscillator (LO) frequency and hoping for good cancellation of the ripple, we set the LO frequency to a number  $N$  of different values so that we can *evaluate* the RF power spectrum and the IF gain spectrum as distinct entities using a least-squares technique; we call this *Least-Squares Frequency Switching*, or *LSFS*. We begin in §2 by reviewing the conventional switching techniques; these introduce extra noise and baseline artifacts, both of which are reduced or eliminated by LSFS.

The rest of the paper is devoted to LSFS. §3 describes the basics of the technique. §4 illustrates our first observational attempt, in which we created a large contiguous bandwidth by aligning three smaller bandwidths end-to-end. The method relies on choosing sensible LO frequencies, and with unwise choices the least-squares matrices can be degenerate; §5 discusses this problem and its solution using Singular Value Decomposition. §7 presents several schemas for choosing LO frequencies, and §8 presents the results of numerical experiments that evaluate the quality of these schemas. Up to this point, all of the discussion is directed towards total power in a single polarization, or alternatively Stokes  $I$ ; §10 shows how the technique applies to the polarized Stokes parameters  $(Q, U, V)$ . Finally, §11 compares switching with LSFS and §12 is a summary.

## 2. REVIEW OF FUNDAMENTALS: POSITION AND FREQUENCY SWITCHING

In heterodyne spectroscopy, we convert the radio-frequency (RF) spectrum to a low intermediate frequency (IF). This conversion is done by multiplying RF power by the local oscillator (LO) in the mixer. Symbolically, denoting frequency by  $f$ , we multiply  $f_{RF}$  by  $f_{LO}$ . This multiplication generates the sum and difference frequencies ( $f_{RF} + f_{LO}$ ) and  $f_{IF} = (f_{RF} - f_{LO})$ ; we remove the sum with a suitable low-pass filter, leaving the desired near-baseband  $f_{IF}$ .

The mixer is a transition point between RF and IF frequencies. We can meaningfully discuss the RF and IF sections as separate entities. Thus, the RF section receives from the sky the antenna temperature  $T_A(f_{RF})$  and also has the receiver contribution  $T_R(f_{RF})$ , which is often much larger. These are multiplied by the RF transfer function, known as the gain  $G_{RF}(f_{RF})$ . Most of the frequency dependence of  $G_{RF}(f_{RF})$  occurs in the feed and electronics, which operates on both  $T_A$  and  $T_R$ , at least to a first approximation. However, often the antenna temperature suffers an additional frequency-dependent gain, which occurs because the incoming power reflects from various portions of the telescope structure and interferes with itself. For simplicity, we neglect this difference and assume that the RF gain affects  $T_A$  and  $T_R$  equally. Thus, symbolically, the RF power into the mixer  $S_{RF}(f_{RF})$  is equal to

$$S_{RF}(f_{RF}) = G_{RF}(f_{RF}) [T_A(f_{RF}) + T_R(f_{RF})] . \quad (1)$$

The IF section has a transfer function, or gain,  $G_{IF}(f_{IF})$ . A well-designed system has no additional power contributed at IF. The spectral power measured by the digital spectrometer is provided as a function of the IF frequency, so the appropriate symbol is  $P_{IF}(f_{IF})$ , which is given by

$$P_{IF}(f_{IF}) = G_{IF}(f_{IF}) S_{RF}(f_{RF}) . \quad (2)$$

The relationship between the spectral channels and IF frequency is fixed. We access different portions of the RF spectrum by changing the LO frequency.

We now break the  $T_A(f_{RF})$  and  $T_R(f_{RF})$  into frequency-independent (“continuum”) and frequency-dependent (“spectral”) portions to simplify further development. With these decompositions, the measured spectral power  $P_{IF}(f_{IF})$  depends on the following quantities:

1.  $T_A(f_{RF})$ . The subscript  $A$  means “antenna temperature”, so this is the spectral line contribution from the *sky*. The explicit presence of the dependence ( $f_{RF}$ ) means that

there is a spectral dependence, as befits a spectral line or the usually slowly-varying continuum radiation.

2.  $T_A$ , the frequency-independent portion of the antenna-temperature continuum contribution. Continuum radiation is weakly dependent on frequency; the frequency-dependent portion is incorporated into  $T_A(RF)$ .
3.  $T_R(f_{RF})$ . The subscript  $R$  means “receiver temperature”, and includes all non-antenna contributions. As with  $T_A(f_{RF})$ , the explicit dependence on  $(f_{RF})$  denotes only the frequency-dependent portion. For many systems, spectral variations in  $T_R(f_{RF})$  are fractionally small.
4.  $T_R$ , the receiver-temperature continuum (frequency-independent) contribution.
5.  $G_{RF}(f_{RF})$ , the RF gain (dependent only on RF frequency). For many systems,  $G_{RF}(f_{RF})$  varies slowly with frequency.
6.  $G_{IF}(f_{IF})$ , the IF gain (dependent on IF frequency). With digital spectroscopy, we must limit the bandwidth by an appropriate IF bandpass filter. This means that  $G_{IF}$  varies severely across the band, varying from 0 to full gain.

With these definitions equation 1 becomes a bit more elaborate. When we look at a source in the sky we measure the on-source (ON) spectrum

$$P(f_{IF}) = G_{IF}(f_{IF}) G_{RF}(f_{RF}) [(T_A(f_{RF}) + T_A) + (T_R(f_{RF}) + T_R)] . \quad (3)$$

Our goal is to disentangle the sky contribution from everything else, i.e. to obtain  $(T_A(f_{RF}) + T_A)$ . Being primarily interested in spectroscopy, a modified goal is to obtain only the spectral portion  $T_A(f_{RF})$ .

We cannot do either of these without dealing with the two gains and the contributions from  $T_R$ . It is traditional to deal with these extraneous quantities by taking a reference spectrum, usually denoted the off-source (OFF) spectrum, and arithmetically combining it with the ON spectrum by taking  $(\frac{ON-OFF}{OFF})$ . This process is commonly known as “switching”. It works well if the frequency dependencies of the extraneous quantities are benign, but this is not always the case. Let us examine the results of this switching process.

Below we consider two ways of obtaining the OFF, one by moving off in position and one by moving off in frequency. Let *primed* quantities indicate the OFF measurements and *unprimed* the ON. Further, let us simplify the problem by assuming the spectral dependence of the receiver temperature to be small, i.e.

$$T_R(f_{RF}) \ll T_R. \quad (4)$$

This allows us to make a Taylor expansions of the expression  $\left(\frac{ON-OFF}{OFF}\right)$  for the two types of switching by dropping terms higher than first order. (We make these expansions to minimize complication; if higher-order terms are included, the expressions become more complicated but the techniques can be still applied).

### 2.1. Position Switching

When the astronomical source is limited in angular extent we can obtain the OFF spectrum by pointing the telescope away from the source. For simplicity, we further assume that the OFF position has no line. Remembering that  $T_R = T'_R$ , this gives for  $\frac{ON-OFF}{OFF}$

$$\frac{P(f_{IF}) - P'(f_{IF})}{P'(f_{IF})} = [T_A(f_{RF}) + (T_A - T'_A)] \left[ \frac{1 - \frac{T_R(f_{RF})}{(T'_A + T_R)}}{T'_A + T_R} \right]. \quad (5)$$

This gives the desired quantity  $T_A(f_{RF})$  plus the additive constant  $(T_A - T'_A)$ , which is the difference between the antenna temperatures of the two positions. The result is further contaminated by the right-hand multiplicative factor. In effect, this is a frequency-dependent gain. However, its effect on the line shape is small because of our assumption of equation 4. These small effects mean that position switching is usually the technique of choice.

However, this does not mean that position switching always provides good results. If the difference in continuum temperatures  $(T_A - T'_A)$  is large, then its multiplication by the right-hand multiplicative factor produces a large effect, and this can make it impossible to distinguish the astronomical spectral line  $T_A(f_{RF})$ . Thus, position switching can fail for weak lines with strong continuum sources.

### 2.2. Frequency Switching

If the spectral line is sufficiently spatially extended then we cannot position switch. The prime example is Galactic HI. Here one normally moves off in frequency. This means that the ON and OFF RF frequencies differ, i.e.  $f_{RF} \neq f'_{RF}$ . In particular, the RF gains differ between the ON and OFF measurements; also, the continuum antenna and receiver

temperatures subtract out, i.e.  $T_A = T'_A$  and  $T_R = T'_R$ . Again, to simplify, we assume the ON (unprimed) and OFF (primed) gains do not differ much, i.e. we define

$$\frac{\Delta G}{G} = 1 - \frac{G'_{RF}(f_{RF})}{G_{RF}(f_{RF})} \quad (6a)$$

and assume

$$\frac{\Delta G}{G} \ll 1. \quad (6b)$$

The differing gains introduce a further complication into the Taylor expansion:

$$\frac{P(f_{IF}) - P'(f_{IF})}{P'(f_{IF})} = \left[ T_A(f_{RF}) + (T_R(f_{RF}) - T'_R(f_{RF})) + \frac{\Delta G}{G}(T_A + T_R + T_A(f_{RF})) \right] \left[ \frac{1 - \frac{T_R(f_{RF})}{(T_A + T_R)}}{T_A + T_R} \right]. \quad (7)$$

This is similar to equation 5 except for the additive term  $\frac{\Delta G}{G}(T_A + T_R + T_A(f_{RF}))$  in the first factor on the right-hand side. Even though  $\frac{\Delta G}{G} \ll 1$ , this term is disastrous because it operates on  $T_R$ , which is large. Unless  $\frac{\Delta G}{G} \lll 1$ , this combination produces serious baseline contamination in frequency switching. Nevertheless, frequency switching works well when, as is often the case,  $\frac{\Delta G}{G}$  varies smoothly and slowly with  $f_{RF}$  so that it is well-represented by a low-order polynomial fit.

### 3. DETERMINATION OF $G_{IF}(f_{IF})$ BY LEAST-SQUARES FREQUENCY SWITCHING (LSFS)

The classical approaches of position and frequency switching work only under good conditions. The quantity having the most severe frequency variations is  $G_{IF}(f_{IF})$ . If we could determine this quantity explicitly we could forgo the switching and, instead, simply divide all measured spectra  $P(f_{IF})$  by  $G_{IF}(f_{IF})$ . Least-squares frequency switching (LSFS) does this explicit determination.

#### 3.1. The Basic Equations and their Iterative Solution

We begin by rewriting equation 3 in a much simpler form. Its right-hand side is the product of the IF gain and several RF quantities. We lump these RF quantities into a single

one,  $S_{RF}(f_{RF})$ :

$$S_{RF}(f_{RF}) = G_{RF}(f_{RF}) [(T_A(f_{RF}) + T_A) + (T_R(f_{RF}) + T_R)] \quad (8)$$

so we rewrite equation 3 as

$$P(f_{IF}) = G_{IF}(f_{IF}) S_{RF}(f_{RF}) . \quad (9)$$

Our technique extracts  $G_{IF}(f_{IF})$  and  $S_{RF}(f_{RF})$  as separate entities.

To proceed, we first express frequencies as channel offsets. The digital spectrometer produces a spectrum having  $I$  channels, with channel number  $i$  ranging from  $i = 0$  to  $i = I - 1$ . The frequency separation between adjacent channels is  $\Delta f$ . Thus, for the IF frequency of channel  $i$  we can write

$$f_{IF,i} = f_0 + i\Delta f , \quad (10)$$

where  $f_0$  is a constant. The separation  $\Delta f$  also applies to  $f_{RF}$ , so apart from a possible additive constant we have for the RF frequency of channel  $i$

$$f_{RF,i} = f_0 + f_{LO} + i\Delta f , \quad (11)$$

where  $f_{LO}$  is the LO frequency.

In LSFS, we make measurements at  $N$  different LO frequencies, each designated by  $n$ . We increment these frequencies in units of  $\Delta f$ , and we write

$$f_{LO,n} = f_{LO,n=0} + \Delta i_n \Delta f , \quad (12)$$

where  $n$  ranges from 0 to  $N - 1$ .  $\Delta i_n$  is the number of channels that  $f_{LO,n}$  is offset from  $f_{LO,n=0}$ ; clearly,  $\Delta i_{n=0} = 0$ . For convenience we assume  $\Delta i_n$  to increase monotonically with  $n$ , so the maximum LO excursion is  $\Delta i_{N-1}$ . We can write all frequencies in units of the channel separation  $\Delta f$ , so the RF frequencies become expressed as digital indices  $i + \Delta i_n$ , where  $i$  is the IF frequency offset from spectral channel zero and  $\Delta i_n$  is the LO frequency offset from the lowest LO frequency (at  $n = 0$ ), both in units of the channel width  $\Delta f$ . Equation 9 becomes

$$P_{i,\Delta i_n} = G_i S_{i+\Delta i_n} . \quad (13)$$

§3.3 presents the simplest “textbook” example, including a figure, to help explain the somewhat confusing relationships embodied in the above description.

There are  $NI$  of these equations. We could use them as our equations of condition for the least-squares fit. However, for reasons discussed below, we normalize the variables for computational efficiency. To normalize, we require the means over  $(i, n)$ , denoted by  $\langle P_{i,\Delta i_n} \rangle$  and  $\langle S_{i+\Delta i_n} \rangle$ , to equal unity; of course, this implies that the typical  $G_i \sim 1$ . Henceforth we assume  $P$  and  $S$  to be so normalized.

In addition, we express  $S_{i+\Delta i_n}$  (whose mean is unity) as an offset  $s_{i+\Delta i_n}$  from unity, i.e. we write

$$S_{i+\Delta i_n} = 1 + s_{i+\Delta i_n} . \quad (14)$$

Clearly, the mean  $\langle s_{i+\Delta i_n} \rangle = 0$ . Below we will assume  $s \ll 1$ , which should be valid as long as the total fractional bandwidth  $\frac{[(I-1)+\Delta i_{N-1}]\Delta f}{\langle f_{RF} \rangle}$  is not too large and, also, there are no strong spectral lines. This assumption will be made only for reasons of computational efficiency and does not affect the final solution. For  $P_{i,\Delta i_n}$ , we can replace the index  $\Delta i_n$  by the index  $n$  to reduce clutter. Equation 13 becomes

$$P_{i,n} = G_i + G_i s_{i+\Delta i_n} . \quad (15)$$

The  $P_{i,n}$  are measured quantities and the  $G_i$  and  $s_{i+\Delta i_n}$  are unknowns to be determined by a least-squares fit. With  $I$  spectral channels,  $N$  LO frequencies, and a maximum LO excursion of  $\Delta i_{N-1}$  frequency channels, the total number of unknowns is  $a = (2I + \Delta i_{N-1})$ : there are  $I$  unknown values of  $G$  and  $(I + \Delta i_{N-1})$  values of  $s$ . For example, for the calibration spectrum of Arecibo’s GALFA spectrometer (Stanimirović et al. 2006), we have 512 channels so  $I = 512$  and we use  $\Delta i_{N-1} = 31$ , so there are 1055 unknowns. This is a substantial, but hardly impossible, least squares problem. Its solution requires, in essence, the inversion of a  $1055 \times 1055$  matrix.

We must solve this set of equations using nonlinear least-squares techniques, which are required because both  $G$  and  $s$  are unknown. Nonlinear least-squares is an iterative process, involving making a guess for the parameters and solving for the difference between the guesses and the true values. Let the guessed values of the parameters be denoted by the



superscript  $g$ . Then, taking the difference between the true values and the guessed values, and using equation 15, we have

$$P_{i,n} - P_{i,n}^g = (G_i + G_i s_{i+\Delta i_n}) - (G_i^g + G_i^g s_{i+\Delta i_n}^g) \quad (16)$$

We express the differences between quantities with the symbol  $\delta$ ; thus the unknowns become  $\delta G_i = G_i - G_i^g$  and  $\delta s_{i+\Delta i_n} = s_{i+\Delta i_n} - s_{i+\Delta i_n}^g$ . As usual in iterative schemes, we assume these differences are small and drop second order terms. Also, we divide through by  $G_i^g$ , an act which implicitly assumes that its fractional error is small, but as we shall see in fact it does not matter if its fractional error isn't small. This gives

$$\frac{\delta P_{i,n}}{G_i^g} = \frac{\delta G_i}{G_i^g} (1 + s_{i+\Delta i_n}^g) + \delta s_{i+\Delta i_n} \quad (17)$$

We have turned the nonlinear least-squares problem into an iterative linear one.

However, the presence of the term  $s_{i+\Delta i_n}^g$  means that the equation-of-condition matrix changes from one iteration to the next. The number of unknowns is large, and the need to evaluate the inverse matrix for each iteration requires significant computational time. We can eliminate this burden by dropping the term  $s_{i+\Delta i_n}^g$  in the above equation. This yields our final set of equations, in which the two unknowns for each channel ( $i$ ) and each LO setting ( $\Delta i_n$ ) are now  $\frac{\delta G_i}{G_i^g}$  and  $\delta s_{i+\Delta i_n}$ :

$$\frac{\delta P_{i,n}}{G_i^g} = \frac{\delta G_i}{G_i^g} + \delta s_{i+\Delta i_n} \quad (18)$$

We use this in an iterative solution in which each step is a linear least-squares fit for the two sets of unknowns. The coefficients of the unknowns are all equal to unity, so they remain constant from one iteration to the next; in other words, the equation-of-condition matrix in the least-squares treatment does not change from one iteration to the next.

Now, it might seem that the elimination of the term  $s_{i+\Delta i_n}^g$  is an arbitrary action that produces erroneous results. However, this is not a problem. As  $\frac{\delta G_i}{G_i^g} \rightarrow 0$ —i.e., as we attain convergence—this term goes to zero so the final solution is unaffected. And, miraculously, it *does* converge—usually rapidly.

The set of equations 18 does not sufficiently constrain the solution. One more equation is needed to keep the mean RF power  $\langle S \rangle$  approximately constant (i.e., approximately equal to unity), which we include as an additional equation of condition:

$$\sum_{i,n} \delta s_{i+\Delta i_n} = 0 \quad (19)$$

To solve this set of equations iteratively, we begin with initial guesses  $G_i^g = 1$  and  $s_{i+\Delta i_n}^g = 0$ . This provides the initial  $P_{i,n}^g = 1$ . We least-squares solve the  $NI$  equations 18 and the equation 19 for the unknowns, which are  $\frac{\delta G_i}{G_i^g}$  and  $\delta s_{i+\Delta i_n}$ . The solution provides the new guesses  $G_i^g$  and  $s_{i+\Delta i_n}^g$ . We usually obtain convergence in  $\sim 10$  iterations, which takes a fraction of a second on a contemporary laptop computer for  $NI = 1055$ .

One final comment. After the calculation is finished, the mean of the gains  $\langle G_i^g \rangle = \mathcal{G}$  ends up departing a bit from unity. For many purposes, e.g. when combining independent LSFS results, it is desirable to scale the gains so that their mean is unity. To accomplish this, simply divide all the derived gains by  $\mathcal{G}$ , i.e. we write

$$G_{i,scaled} = \frac{G_i^g}{\mathcal{G}} . \quad (20a)$$

Similarly, the RF powers are also scaled:

$$S_{i+\Delta i_n,scaled} = \mathcal{G} (1 + s_{i+\Delta i_n}^g) . \quad (20b)$$

### 3.2. Number of Equations of Condition; Number of Unknowns

In least-squares fitting we develop equations of condition, one for each observed quantity. Least-squares fitting requires the unknowns to be overdetermined, i.e. the number of unknowns to be smaller than the number of equations of condition. As mentioned above just after equation 15, the number of unknowns is  $a = (2I + \Delta i_{N-1})$ . The number of equations of condition is  $M = NI + 1$ :  $I$  channels for each of the  $N$  LO frequencies, plus equation 19. For the least-squares technique we require  $M > a$ , i.e.

$$NI > 2I + \Delta i_{N-1} - 1 . \quad (21)$$

Clearly, it makes no sense to have  $\Delta i_{N-1} > I$ , because that generates additional values of  $s_{i+\Delta i_n}$  while providing no information on  $G_i$ . Thus we require  $\Delta i_{N-1} = hI$ , where  $h < 1$ . This yields

$$N > 2 + h - \frac{1}{I} \quad (22)$$

With  $h < 1$ , we generally require  $N \geq 3$ . The quantity  $h$  is maximum LO separation  $\Delta i_{N-1}$  in units of the IF bandwidth; we refer to  $h$  as the *fractional LO coverage*.

### 3.3. An Illustrative Textbook Example

We present an illustrative example with the goal of clarifying the procedure. The simplest example has the smallest numbers. Since we need  $N \geq 3$  and  $I > \Delta i_{N-1}$ , we choose  $I = 4$  and  $N = 3$ , with  $\Delta i_n = [0, 1, 3]$ . That is, we have a 4-channel spectrometer. We use 3 LO frequencies, with the latter two spaced by 1 and 3 channels from the first. This provides an arithmetic progression for the successive frequency differences  $\Delta i_{nn'}$ , which we define as  $(\Delta i_n - \Delta i_{n'})$  (where we consider all combinations of  $n$  and  $n'$ ). The values of  $\Delta i_{nn'} = [0, 1, 2, 3]$ . Note that  $\max(\Delta i_{nn'}) = \Delta i_{N-1} = 3$ . Figure 1 graphically illustrates these parameters; this Figure assumes  $G_{IF}(f_{IF}) = 1$  everywhere.

In matrix form, the equations of condition (equations 18 and equation 19) are

$$\mathbf{X} \cdot \mathbf{a} = \mathbf{p} . \quad (23)$$

Here,  $\mathbf{X}$  has  $(NI + 1)$  rows and  $(2I + \Delta i_{N-1})$  columns,  $\mathbf{a}$  is the  $(2I + \Delta i_{N-1})$  vector of unknowns, and  $\mathbf{p}$  is the  $(NI + 1)$  vector of  $NI$  measured and one constrained quantities. Our notational convention is that boldface small letters are vectors and boldface large letters are matrices.

For our textbook example, in the vector of unknowns  $\mathbf{a}$ , to avoid clutter we write  $g_i$  in place of  $\frac{\delta G_i}{G_i^g}$ . To save space, we write the transpose of this vector, which is

$$\mathbf{a}^T = [g_0, g_1, g_2, g_3, \delta s_0, \delta s_1, \delta s_2, \delta s_3, \delta s_4, \delta s_5, \delta s_6] . \quad (24)$$

In the vector of measured quantities  $\mathbf{p}$ , we write  $p_{i,n}$  in place of  $\frac{\delta P_{i,n}}{G_i^g}$ . This vector's transpose is

$$\mathbf{p}^T = [p_{0,0}, p_{1,0}, p_{2,0}, p_{3,0}, p_{0,1}, p_{1,1}, p_{2,1}, p_{3,1}, p_{0,2}, p_{1,2}, p_{2,2}, p_{3,2}, 0] , \quad (25)$$

and the equation-of-condition matrix consists of the coefficients in equations 18 and 19, all

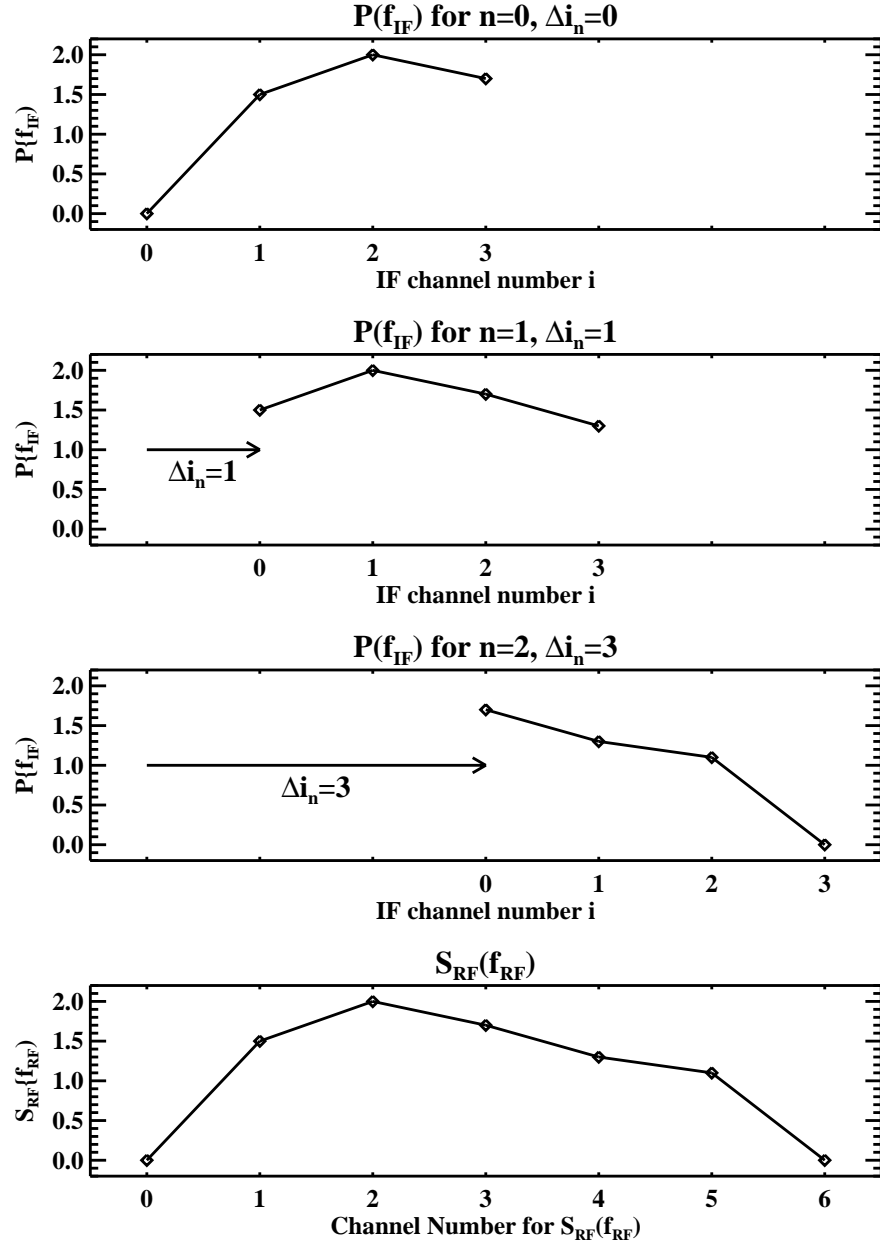


Fig. 1.— Graphical illustration of the illustrative textbook example, assuming all  $G_{IF}(f_{IF}) = 1$ . The top three panels show the measured IF power  $P_{i,\Delta i_n}$  [which is captioned “ $P(f_{IF})$ ”] versus IF channel number  $i$ ; the bottom panel shows the RF spectrum  $S_{i+\Delta i_n}$  [which is captioned “ $S_{RF}(f_{RF})$ ”] versus  $(i + \Delta i_n)$  (which is captioned “Channel Number for  $S_{RF}(f_{RF})$ ”).

of which are unity:

$$\mathbf{X} = \begin{bmatrix} 1 & 0 & 0 & 0 & 1 & 0 & 0 & 0 & 0 & 0 & 0 & 0 \\ 0 & 1 & 0 & 0 & 0 & 1 & 0 & 0 & 0 & 0 & 0 & 0 \\ 0 & 0 & 1 & 0 & 0 & 0 & 1 & 0 & 0 & 0 & 0 & 0 \\ 0 & 0 & 0 & 1 & 0 & 0 & 0 & 1 & 0 & 0 & 0 & 0 \\ 1 & 0 & 0 & 0 & 0 & 1 & 0 & 0 & 0 & 0 & 0 & 0 \\ 0 & 1 & 0 & 0 & 0 & 0 & 1 & 0 & 0 & 0 & 0 & 0 \\ 0 & 0 & 1 & 0 & 0 & 0 & 0 & 1 & 0 & 0 & 0 & 0 \\ 0 & 0 & 0 & 1 & 0 & 0 & 0 & 0 & 1 & 0 & 0 & 0 \\ 1 & 0 & 0 & 0 & 0 & 0 & 0 & 1 & 0 & 0 & 0 & 0 \\ 0 & 1 & 0 & 0 & 0 & 0 & 0 & 0 & 1 & 0 & 0 & 0 \\ 0 & 0 & 1 & 0 & 0 & 0 & 0 & 0 & 0 & 1 & 0 & 0 \\ 0 & 0 & 0 & 1 & 0 & 0 & 0 & 0 & 0 & 0 & 1 & 0 \\ 0 & 0 & 0 & 0 & 1 & 1 & 1 & 1 & 1 & 1 & 1 & 1 \end{bmatrix} . \quad (26)$$

In this matrix,

1. The first four rows pertain to the lowest LO frequency with  $\Delta i_0 = 0$
2. The next two pairs of four rows pertain to  $\Delta i_1 = 1$  and  $\Delta i_2 = 3$ .
3. The last row is the power conservation equation 19.
4. The first four columns are the coefficients of the four IF gains  $\frac{\delta G_i}{G_i^g}$  in equation 18.
5. The last seven columns are the coefficients of the seven RF powers  $\delta s_{i+\Delta i_n}$  in equation 18.

The usual least-squares process of solving these equations of condition (see Press et al. 1992) involves multiplying  $\mathbf{X}$  by its transpose to obtain the curvature matrix (the matrix of normal equations) and then taking the inverse of that matrix product to obtain the covariance matrix  $\boldsymbol{\alpha}$ :

$$\boldsymbol{\alpha} = (\mathbf{X}^T \cdot \mathbf{X})^{-1} , \quad (27)$$

and the solution for the coefficient vector is

$$\mathbf{a} = (\boldsymbol{\alpha} \cdot \mathbf{X}^T) \cdot \mathbf{p} . \quad (28)$$

For this illustrative problem, the inverse is well defined with no numerical problems. The biggest normalized covariance (or correlation), obtained by converting the covariance matrix to a correlation matrix, is  $-0.51$ , whose absolute value is not unreasonably large.

#### 4. AN ILLUSTRATIVE REAL-WORLD EXAMPLE

Our initial experiments with LSFS were performed with three independent banks of Arecibo’s interim correlator<sup>1</sup>. Each bank had 2048 channels and covered a bandwidth of 25 MHz; we overlapped the three banks by cutting off 64 channels on each end, i.e. we spaced the centers by  $\frac{31}{32} \times 25$  MHz, stitching together a single spectrometer with 5888 channels covering a total contiguous bandwidth of 71.875 MHz. We binned the channels by a factor of 8, making 736 channels of width 0.0977 MHz. We used four different LO frequencies with spacings  $\Delta i_n = [0, 35.50, 43.69, 72.36]$ , providing the nonuniform set of six spacings  $\Delta i_{nn'} = [8.19, 28.67, 35.50, 36.86, 43.69, 72.36]$ . Figure 2 shows the results.

LSFS works reasonably well in this initial-experiment example. We performed this observation before devising the schemas discussed in §7 and we cannot remember how we chose the set of LO frequencies  $\Delta i_n$ , but we suspect it is not a very good choice because the middle third of the RF power spectrum  $S_{RF}(f_{RF})$  is slightly displaced from the others. Such artifacts do not occur with the better schemas of §7. It is clear that LSFS would perform admirably with a better schema, and this particular case illustrates how one can accomplish the often desirable goal of reliably generating a contiguous large band from narrower ones.

We refer to two other real-world examples. In one, we use LSFS to determine  $G_{IF}(f_{IF})$  and use that gain spectrum to correct thousands of measured spectra; we provide some details in §5.3. In the other, we use LSFS to determine the intrinsic ripples in the RF power spectrum; see §11.2.

### 5. DETAILS OF MATRIX ALGEBRA FOR LARGER $I$ , LARGER $N$

#### 5.1. Degeneracy in the $\mathbf{X}$ Matrix

Under some conditions we find empirically that some of the equations of condition become degenerate. This degeneracy is best understood by considering the  $\mathbf{X}$  matrix in

---

<sup>1</sup>The Arecibo Observatory is part of the National Astronomy and Ionosphere Center, which is operated by Cornell University under a cooperative agreement with the National Science Foundation.

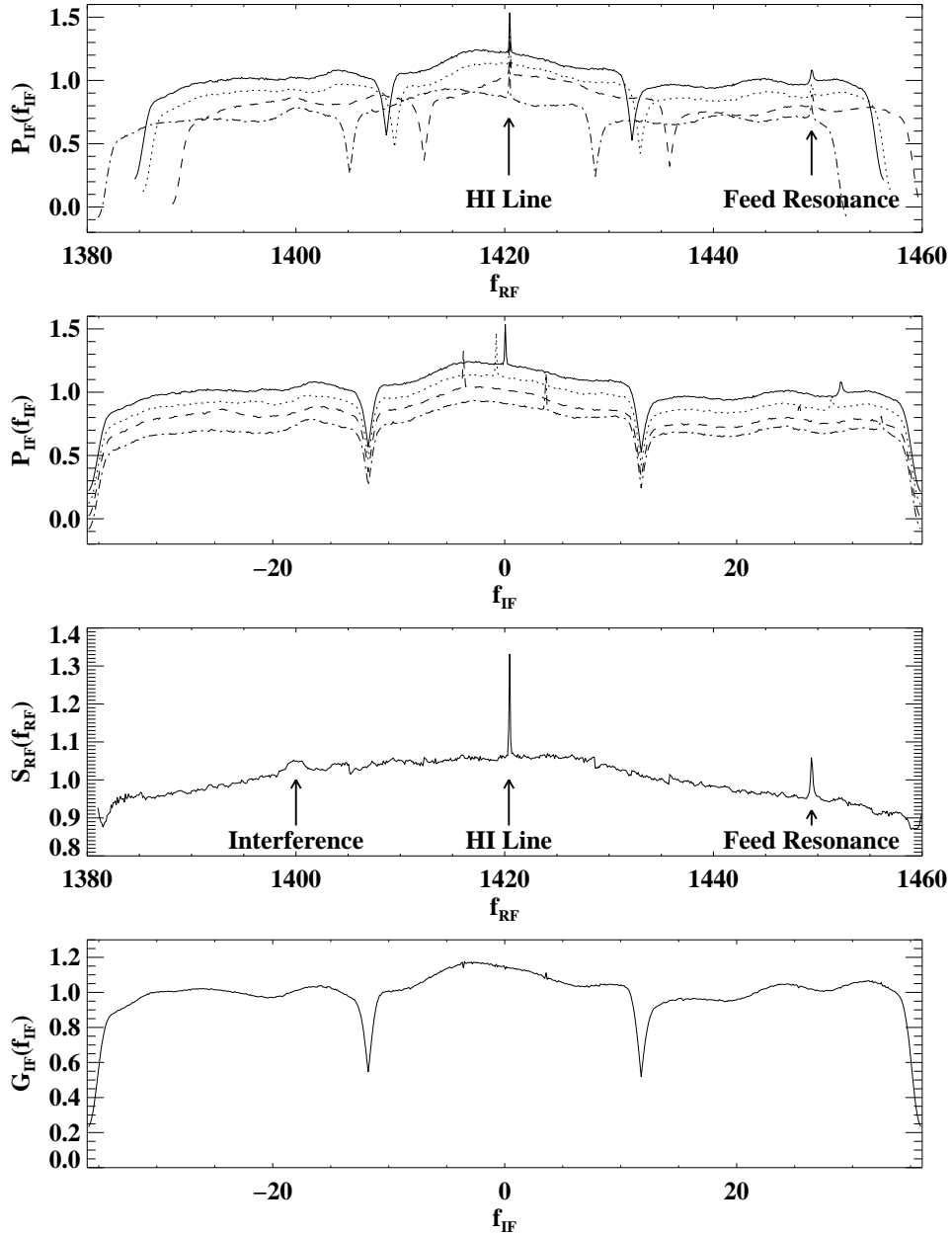


Fig. 2.— Real-world example of LSFS discussed in §4. The top panel shows the total measured power  $P_{IF}(f_{IF})$  versus RF frequency for the four LO frequencies; note that the HI line remains fixed near 1420 MHz and the IF bandpass shapes move with the LO. The second panel shows the measured power  $P_{IF}(f_{IF})$  versus IF frequency for the four LO frequencies; the IF bandpass shapes remain fixed and the HI line moves with the LO. The third panel shows the derived RF power,  $S_{RF}(f_{RF})$  in equation 9, with the known spectral peaks identified. The bottom panel shows the IF gain  $G_{IF}(f_{IF})$ .

equation 23 as a series of  $a$  column vectors, where  $a$  is the number of unknowns;  $a = 2I + \Delta i_{N-1}$ . Suppose that two columns are degenerate, meaning that they are linear combinations of each other. In the matrix product  $\mathbf{X} \cdot \mathbf{a}$ , there is a one-to-one relationship between each column in  $\mathbf{X}$  and its corresponding unknown coefficient in  $\mathbf{a}$ . A degeneracy between two columns means that the matrix product cannot distinguish between the two corresponding coefficients.

When one applies the usual technique of generating the normal equations and inverting the curvature matrix, as in equation 27, it does not work: the inverse matrix does not exist because of the degeneracy. In cases like this one has two choices: think hard and find the root cause of the degeneracies; or use Singular Value Decomposition (SVD) to empirically remove them. The number of unknowns is large, so the first option—picking through a huge matrix looking for degeneracies—is difficult, probably even for a mathematical expert. Therefore, we choose the latter one.

## 5.2. SVD: Theory

Numerical Recipes (Press 1992) provides a useful discussion of the SVD technique as applied to least squares. The SVD technique forgoes the usual generation of the normal equations for calculating the matrix  $(\boldsymbol{\alpha} \cdot \mathbf{X}^T)$  in equation 28. Rather, it expresses this matrix in terms of three matrices that are derived from the SVD decomposition of the  $\mathbf{X}$  matrix.

The cornerstone of SVD is that any  $M \times a$  matrix, where the number of rows  $M$  and the number of columns  $a$  satisfy  $M \geq a$ , can be decomposed as the product of three matrices. In particular, our matrix  $\mathbf{X}$  in equation 23 satisfies this criterion, so we can write

$$\mathbf{X} = \mathbf{U} \cdot [\mathbf{W}] \cdot \mathbf{V}^T, \quad (29)$$

where the right-hand side contains the three SVD matrices. These matrices have important properties:

1.  $\mathbf{U}$  is  $M \times a$ ,  $[\mathbf{W}]$  is  $a \times a$  and diagonal, and  $\mathbf{V}^T$  is  $a \times a$ . The square brackets around the matrix  $\mathbf{W}$  indicate that it is diagonal.
2. The columns of  $\mathbf{U}$  consist of unit vectors that are orthonormal, and the same is true for  $\mathbf{V}$ . Because  $\mathbf{V}$  is square, its rows are also orthonormal so that  $\mathbf{V} \cdot \mathbf{V}^T = 1$ . Recall that, for square orthonormal vectors, the transpose equals the inverse so  $\mathbf{V}^T = \mathbf{V}^{-1}$ .



Degeneracies are directly reflected in the  $\mathbf{V}$  and  $[\mathbf{W}]$  matrices. The square matrix  $\mathbf{V}$  consists of a set of  $a$  orthonormal column vectors. These are normalized orthogonal vectors that are linear combinations of *non*orthogonal column vectors in  $\mathbf{X}$ . Suppose that  $L$  columns of  $\mathbf{X}$  are degenerate. Then the number of independent orthonormal vectors represented in  $\mathbf{X}$  is decremented by  $L$ . Nevertheless, the  $\mathbf{V}$  matrix still contains  $a$  independent orthonormal vectors. The decrement by  $L$  is represented not by the orthonormal column vectors in  $\mathbf{V}$ , but rather by their *weights* in the diagonal matrix  $[\mathbf{W}]$ . Each column vector in  $\mathbf{V}$  has an associated weight in  $\mathbf{W}$ , and if there is degeneracy, then the corresponding value of  $\mathbf{W}$  is zero. This means the corresponding orthonormal vector in  $\mathbf{V}$  cannot be represented by the column vectors in  $\mathbf{X}$ .

Having derived the SVD components of  $\mathbf{X}$ , we can write for the matrix product  $(\boldsymbol{\alpha} \cdot \mathbf{X}^T)$  in equation 28

$$(\boldsymbol{\alpha} \cdot \mathbf{X}^T) = \mathbf{V} \cdot \left[ \frac{\mathbf{1}}{\mathbf{W}} \right] \cdot \mathbf{U}^T . \quad (30)$$

Now suppose there is degeneracy; then the corresponding values of  $[\mathbf{W}]$  are zero, so the corresponding values of  $[\frac{\mathbf{1}}{\mathbf{W}}]$  become infinite. This is an attempt by the matrix algebra to represent the space defined by the corresponding columns of  $\mathbf{V}$  with data that were taken with inappropriate values of  $\mathbf{X}$ .

SVD, as applied to least squares, handles these infinities by setting the corresponding values of  $[\frac{\mathbf{1}}{\mathbf{W}}]$  (which are formally equal to  $\infty$ ) to zero. This provides stable, realistic solutions in which the offending degenerate coefficient values are close to being correct—or, at least, not being totally unreasonable. By following this procedure, one can handle degeneracies without understanding their cause simply by zeroing out the relevant components of the  $[\frac{\mathbf{1}}{\mathbf{W}}]$  vector.

This zeroing process can—and should—be applied in cases of *near* degeneracy. Just exactly what “near” means depends on the noise in the data, because the data values are amplified by  $[\frac{\mathbf{1}}{\mathbf{W}}]$  in calculating the coefficient values. For sufficiently noisy data one might best zero out the offending elements of  $[\frac{\mathbf{1}}{\mathbf{W}}]$  even if they are not too terribly large.

The  $\mathbf{X}$  matrix depends only on the values  $\Delta i_n$ , not on the data values  $S$ . Moreover, calculating the inverse of the  $\mathbf{X}$  matrix is computationally expensive. Thus, when using a particular set of LO frequency offsets for multiple observations, it behooves one to do the SVD calculation of  $(\boldsymbol{\alpha} \cdot \mathbf{X}^T)$  once, store the results on disk, and read them back when necessary. This has the further advantage that one can examine the weight vector  $[\mathbf{W}]$  once for each set of LO frequency offsets, decide which particular values of  $[\frac{\mathbf{1}}{\mathbf{W}}]$  to set to zero, and

forget about dealing with this on a case-by-case basis. Section 5.3 provides some comments on examples we encountered.

### 5.3. SVD: Practice

The ratio of maximum to minimum weights determines whether some inverse weights should be zeroed. For noise-free data, ratios that come close to the machine accuracy (perhaps  $10^6$  for single-precision math) should be zeroed; in the presence of noise, smaller ratios should be zeroed. Our initial experiment of §4 with four LO frequencies had no degeneracy. For our numerical experiments, we examined various schemas, which are detailed in §7.1 and §7.2. Most schemas had weight ratios smaller than 2500. The highest ratios occurred for  $N=3$  and decreased rapidly (e.g., by a factor of 2) for successive increases in  $N$ . In some cases we zeroed inverse weights to keep the ratio smaller than a few hundred, and in some cases not.

There were two exceptions, which had much larger ratios. The MRN,R schemas had large ratios, again  $\sim 10^7$ , for  $R \neq 1$ . For  $R = 2, 4, \text{ and } 8$  we had to zero 1, 3, and 7 inverse weights, respectively. (Recall that this is out of a total of over 1000 weights). The  $2^{MRN}$  schema had ratios  $\sim 10^7$  for a few elements; this schema is no good anyway and we do not quote results for it here.

Our work with the GALFA spectrometer (Stanimirović et al. 2006) is an interesting case. This spectrometer observes two spectra simultaneously, the wide “calibration” spectrum and the much narrower “science” spectrum. The calibration spectrum is 100 MHz wide with 512 channels, for which we use the MR7 arrangement (see §7), exactly like our MR7 numerical experiment below.

We use the same set of 7 LO frequencies for the science spectrum. This spectrum covers a bandwidth of  $\frac{100}{14} \approx 7.143$  MHz and has 8192 channels, which makes  $\Delta f \approx 872$  Hz. Thus, the LO increment  $\Delta f$  is about 224 times the channel spacing. Of the 8192 channels, 7679 are recorded. We invent an extra, making the total 7680. Before applying LSFS we rebin these, lumping successive bins of 16 together so that the total number of binned channels is 480. The frequency offset of the seventh LO frequency is almost as large as the total bandwidth, so we use only the first six LO frequencies. This gives increments  $\Delta i_{nn'}$  ranging from 14 to 283, so  $h = \frac{283}{480} \approx 0.59$ . We assume smoothness and use an interpolation procedure to recover the 7679 values of  $G_{IF}(f_{IF})$ .

This narrowband case exhibits thirteen degeneracies. We have 1198 coefficients to derive, so we have 1198 orthonormal column vectors in the  $\mathbf{V}$  matrix. The 1198 weights  $[\mathbf{W}]$  range

from about  $8.9 \times 10^{-7}$  to 27. Thirteen weights are nearly degenerate, being smaller than  $1.8 \times 10^{-6}$ ; we set their corresponding inverses to zero. The lowest non-zeroed weight is  $\approx 0.69$ , so there is a huge gap between the range of accepted weights ( $\sim 0.69$  to 27) and the zeroed inverse weights (the largest is  $\sim 1.8 \times 10^{-6}$ ). Zeroing the 13 inverse weights provides a very nice solution for the IF gain, which is used to correct thousands of measured mapping spectra.

## 6. REGARDING COMPUTING TIME

Regarding computing time, we scale from the MR7 scheme described in §7, which has  $I = 512$ ,  $N = 7$ , and  $\Delta i_{N-1} = 31$ . The LSFS  $\mathbf{X}$  matrix *inversion* for  $I = 512$  and  $\Delta i_{N-1} = 31$  takes 123 seconds on a not-quite contemporary laptop computer programmed in IDL. This time scales as the number of unknowns cubed, i.e. as  $(2I + \Delta i_{N-1})^3$ , so for  $I = 4096$  it would take about 20 hours. This is a long time, but as discussed in §3 and §5, the matrix inversion should be done once and the result stored on disk. The  $\mathbf{X}$  matrix is sparse, and perhaps sparse matrix techniques would make its inversion go faster.

Once the matrix is inverted the *solutions* go fast. For the MR7 scheme, the solution time is about 0.6 seconds. This time scales as  $NI(2I + \Delta i_{N-1})$ , so if  $N$  is kept constant it scales roughly as  $I^2$ ; thus, 4096 channels would take about 5 seconds.

## 7. SCHEMAS FOR LO SETTINGS

In §3.2 we found that the number of different LO frequencies,  $N$ , must exceed 3. However, this tells us nothing about how the quality of the solution is affected by  $N$ , and even less about how the LO frequencies should be chosen, i.e. the values of  $\Delta i_n$ . It is not clear to this author how to investigate these matters analytically. Rather, we turn to numerical experiments. Specifically, we consider what we hope are intelligent schemas for  $\Delta i_n$ , adopt them for a range of  $N$ , and analyze the results of the numerical experiments. We begin by discussing various schemas. First we describe a conservative approach, which uniformly samples  $\Delta i_{nn'}$  up to a maximum but requires a fairly large number of  $N$ , and then we describe some less conservative approaches.

### 7.1. The Minimum-Redundancy (MR) Schema

First we discuss Minimum-Redundancy (MR) settings having  $N$  LO settings. We will denote such settings by the symbol MRN, where  $N$  is the number of LO settings. At the most conservative and basic level, common sense suggests the following criteria:

1. An arithmetical progression for the successive frequency differences  $\Delta i_{nn'}$ , which we also call “spacings”. Spacings should begin with unity and increment by unity up to some maximum value  $N_{max}$ . It seems to us, intuitively, that incrementing by unity is akin to sampling uniformly when doing Fourier transforms, which is always the desirable situation.
2. A reasonably large value for the fractional LO coverage  $h$ , which is the maximum LO offset  $\Delta i_{N-1}$  in units of the spectrometer bandwidth. It seems to us, intuitively, that precisely recovering broad-scale frequency structure requires sampling those broad scales with a comparably large value of  $\Delta i_{N-1}$ .

The problem of generating an arithmetic progression with  $N$  settings of the LO frequency is akin, in radioastronomical interferometry, to the well-studied problem of generating an arithmetic progression of unidirectional baselines with a linear array of telescopes. For  $N$  LO frequencies there are  $\frac{N(N-1)}{2}$  frequency spacings, some of which are redundant; similarly, for  $N$  telescopes on the ground there are  $\frac{N(N-1)}{2}$  distance spacings, some of which are redundant. The classic discussion by Moffett (1968) considers these minimum-redundancy telescope arrays, which use  $N$  antennas to generate a minimally redundant arithmetical progressive series for  $\Delta i_{nn'}$ . Zero redundancy is possible only for  $N \leq 4$ ; for  $N = 4$  the spacings range up to  $\Delta i_{N-1} = 6$ . For  $N > 4$  there must be some redundancy. Moffett presents two types of minimum-redundancy arrays, *restricted* and *general*.

Restricted minimum-redundancy arrays provide all spacings  $\Delta i_{nn'}$  up to a maximum  $N_{max}$ , with no gaps; these are useful for radio interferometry when the available real estate is limited. General ones provide all spacings up to a particular limit, and in addition provide larger spacings. For example, the  $N = 7$  restricted array provides all spacings  $\Delta i_{nn'} \leq 17$ , while the  $N = 7$  general array provides all spacings  $\Delta i_{nn'} \leq 18$  and, in addition,  $\Delta i_{nn'} = [24, 26, 31]$ . For our purposes the general array is a better choice: apart from the fact that we are not limited by available real estate, it provides more different values for  $\Delta i_{nn'}$  and, also, a larger value of  $h$ . For the general minimum-redundancy arrays, roughly  $\Delta i_{N-1} \approx 31 \left(\frac{N}{7}\right)^{2.66}$ . This is a steep dependence, so it is possible to generate a large number of LO frequencies to get a desired  $h$  without making  $N$  ridiculously large.

The first nine rows of Table 1 presents information about the range  $N = 3-11$ . Column 1 contains our names for the setting arrangement, running from MR3 to MR11; columns 2-4 provide the three quality indicators from the numerical experiments, which we define below in §8; columns 5-6 provide the maximum LO separation with continuous coverage  $N_{max}$  and the maximum LO separation  $\Delta i_{N-1}$ . The last column, headed “LO spacings”, is from the general arrays in Moffett’s (1968) Table 1. It has dots and numbers: the dots represent the frequency settings of the LO and the numbers the spacing between the frequencies in units of the minimum spacing. Ishiguro (1980) discusses a subset of algorithms that generate arrays having larger  $N$ .

## 7.2. Other Schemas

From the practical standpoint, an observer wants to keep  $N$  as small as possible. MRN settings obtain uniform coverage in  $\Delta i_{nn'}$  but require fairly large  $N$  to attain large maximum separations  $\Delta i_{N-1}$ . Here we propose schemas that sacrifice the uniformly-sampled  $\Delta i_{nn'}$  in favor of increasing the maximum separation  $\Delta i_{N-1}$ .

We consider five such schemas, four of which are specified in terms of the MRN spacings  $\Delta i_{MRN}$ . The five schemas are:

1. The LO separations are the square of the MRN set, equal to  $(\Delta i_{MRN})^2$ . We designate this by  $MRN^2$ . This works quite well and we recommend it in our comparative discussion in §8.3.
2. The LO separations are the 1.7-power of the MRN set, equal to  $(\Delta i_{MRN})^{1.7}$ . We designate this by  $MRN^{1.7}$ . This works almost as well as the  $MRN^2$  schema.
3. The LO separations are equal to  $-3^n$ , where  $n$  varies from 0 to  $N - 1$ . For  $1 \leq n \leq (N - 1)$ , the  $n^{th}$  LO frequency is given by  $\Delta i_n = \Delta i_{n-1} + (-3)^{n-1}$ . We designate this by  $3^{\Delta N}$ . This works comparably to the  $MRN^{1.7}$  schema.
4. The LO *values* (not the separations) are a power-law series. The offset of the  $n^{th}$  LO from the  $0^{th}$  is equal to  $n^{1.7}$ , where  $n$  varies from 0 to  $N - 1$ . We designate this by  $N^{1.7}$ . This works less well than the above schemas.
5. The LO separations are equal to  $2^{\Delta i_{MRN}}$ . We designate this schema by  $2^{MRN}$ . This schema provides such poor results that we do not include it in Table 1.

The exponent 1.7 in schemas  $MRN^{1.7}$  and  $N^{1.7}$  is inspired by the choice of spacings for the Very-Large-Array antennas. We have not experimented with different values of the exponent.

Table 1. Schemas: Definitions and Results

Schema	$\Delta RF$	$\sigma(IF)$	$F\text{-Ampl}[1]$	$N_{max}$	$\Delta i_{N-1}$	LO spacings
MR3	−4.1	4.1	63.4	3	3	·1·2·
MR4	−4.4	3.4	74.1	6	6	·1·3·2·
MR5	0.149	1.19	25.9	9	13	·4·1·2·6·
MR6	0.051	1.27	16.8	13	19	·6·1·2·2·8·
MR7	0.020	1.04	11.2	18	31	·14·1·3·6·2·5·
MR8	0.028	1.07	9.2	24	39	·8·10·1·3·2·7·8·
MR9	0.005	1.04	9.4	29	29	·1·3·6·6·6·2·3·2·
MR10	0.003	0.93	5.2	37	73	·16·1·11·8·6·4·3·2·22·
MR11	0.004	0.99	4.5	45	91	·18·1·3·9·11·6·8·2·5·28·
MR3 <sup>2</sup>	−4.3	2.20	61.6	1	5	·1·4·
MR4 <sup>2</sup>	0.319	1.23	51.9	1	14	·1·9·4·
MR5 <sup>2</sup>	0.012	1.04	5.8	1	57	·16·1·4·36·
MR6 <sup>2</sup>	0.013	1.08	3.1	1	109	·36·1·4·4·64·
MR3 <sup>1.7</sup>	−4.2	2.68	61.2	1	4	·1·3·
MR4 <sup>1.7</sup>	−2.6	1.64	106.3	1	11	·1·6·4·
MR5 <sup>1.7</sup>	0.029	1.10	8.8	1	36	·11·1·3·21·
MR6 <sup>1.7</sup>	0.017	1.14	6.0	1	63	·21·1·3·4·34·
3 <sup>1.7</sup>	−4.1	4.17	62.0	3	3	·1·2·
4 <sup>1.7</sup>	0.451	1.89	48.1	3	6	·1·2·3·
5 <sup>1.7</sup>	0.250	1.28	50.3	7	10	·1·2·3·4·
6 <sup>1.7</sup>	−2.7	1.68	129	11	15	·1·2·3·4·4·
3 <sup>Δ4</sup>	0.223	1.22	32.3	3	9	·2·1·6·
3 <sup>Δ5</sup>	0.021	0.98	10.9	3	27	·18·2·1·6·
3 <sup>Δ6</sup>	0.021	1.17	4.2	3	81	·18·2·1·6·54·
MR5,8-x	0.019	1.64	25.7	8 × 9	8 × 13	8 × [·4·1·2·6·]
MR5 <sup>2</sup> , 8-x	0.011	1.30	5.6	8 × 1	8 × 57	8 × [·16·1·4·36·]
MR7,2	0.068	1.21	5.4	2 × 18	2 × 31	2 × [·14·1·3·6·2·5·]
MR7,4	0.273	4.91	3.0	4 × 18	4 × 31	4 × [·14·1·3·6·2·5·]
MR7,8	7 × 10 <sup>6</sup>	341	5.8	8 × 18	8 × 31	8 × [·14·1·3·6·2·5·]

Note. — Schemas are defined in the text, §7.1 and §7.2. Columns 2-4 contain our three quality indicators: the mean RF power offset and the RMS error for IF gains, defined in §8.1, and the lowest-frequency Fourier amplitude, defined in §8.2. Spacings are completely covered up to  $N_{max}$ , which is given in column 5. Column 6 contains  $\Delta i_{N-1}$ , which is the maximum LO spacing and is equal to the sum of the  $N - 1$  spacings.

## 8. NUMERICAL EXPERIMENTS

We evaluated the above schemas in numerical experiments. We first invented a noise-free IF gain and RF power spectrum and, for each schema, ran 256 trials. In each trial we added 2 K Gaussian-distributed noise for each LO setting.

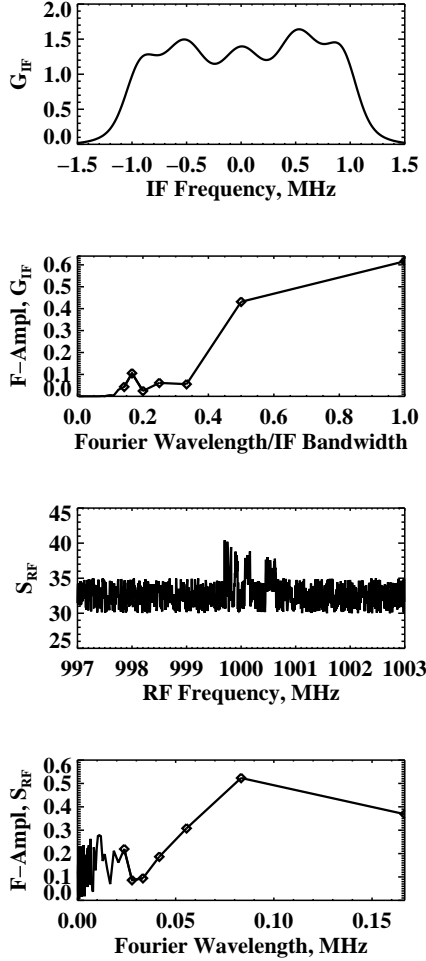


Fig. 3.— The noise-free input spectra for our numerical experiments. The top two panels display the IF gain spectrum versus IF frequency and its Fourier amplitude spectrum; the bottom two the RF power spectrum versus RF frequency and its Fourier amplitude spectrum.

Figure 3 shows the noise-free input spectrum and its Fourier amplitude spectrum for the IF gain (top two panels) and the RF power (bottom two panels). The IF gain is the

product of three terms, which are meant to simulate three different hardware characteristics:

1. The overall shape of the band-limiting filter at the spectrometer input,

$$G_{IF,filter} = 0.5(\tanh[5(f_{IF} + 1)] - \tanh[5(f_{IF} - 1)]) . \quad (31a)$$

2. A standing wave with period 0.5 MHz in the cable connecting the feed to the spectrometer

$$G_{IF,wave} = 1 + 0.1 \cos \left( 2\pi \frac{f_{IF}}{0.5} \right) . \quad (31b)$$

3. A slowly-varying polynomial-dependent gain from electronics and amplifiers

$$G_{IF,poly} = 1 + 0.1f_{IF} + 0.5f_{IF}^2 . \quad (31c)$$

In all of the above, the IF frequency  $f_{IF}$  runs from  $-1.5$  to  $+1.5$  MHz, which range is covered by  $I = 512$  channels. The top panel of Figure 3 shows the product of these terms. The second panel shows the Fourier amplitude spectrum, with the horizontal axis being the Fourier component wavelength in units of the 3-MHz IF bandpass. Thus, the standing wave term above in equation 31b is clear in this plot: its period is 0.5 MHz, which is  $\frac{1}{6}$  the 3-MHz IF bandwidth so it appears at 0.17 on the horizontal axis. We could have labeled the horizontal axis “Fourier Wavelength, MHz” and made the maximum  $\frac{1}{3}$  instead of 1.

Similarly, the RF power is the sum of three terms:

1. A frequency-independent system temperature of 30 K;
2. Five rectangular spectral lines of widths 2, 4, 8, 16, and 32 channels having amplitudes 7, 6, 5, 4, 3 K and spaced so that they are nonoverlapping (we used rectangular lines to facilitate seeing degradation in frequency resolution);
3. Channel-to-channel uniformly-distributed random noise with amplitude limits 0 to 5 K. This simulates a rich, crowded mm-wave spectrum containing a plethora of molecular lines.

The sum of all these components provides a channel-average system temperature of slightly more than 32.5 K. The third panel of Figure 3 shows the RF power over 6 MHz bandwidth. The fourth panel shows the Fourier amplitude spectrum, with the horizontal axis being the Fourier wavelength in units of MHz. That is, sinusoidal ripples across the spectrum in panel 3 have a maximum period of 1 cycle over the 6 MHz band.



### 8.1. Results: Two Quality Indicators

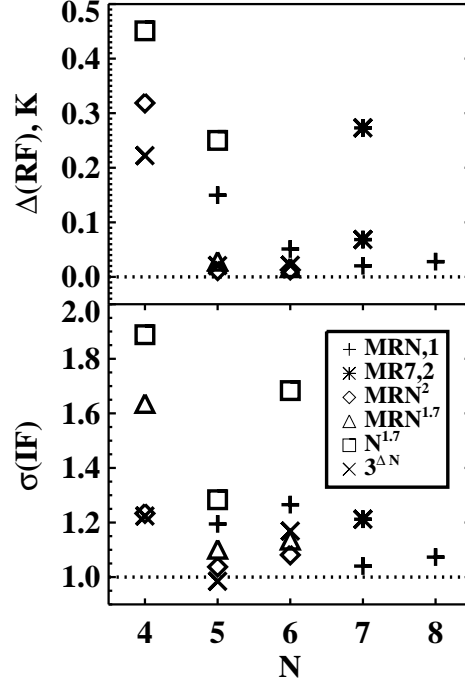


Fig. 4.— Plots of quality indicators  $\Delta(RF)$  and  $\sigma(IF)$  versus the number of LO settings  $N$ . The different plot symbols specify the LO spacing schemas discussed in §7.1 and §7.2. The top panel displays the mean error of the RF power and the bottom the RMS uncertainty of the IF gain.

Figure 4 plots quality indicators for the above schemas as a function of the number of LO settings  $N$ . Also, Table 1 lists these quantities in columns 2 and 3. We first consider two indicators:

1. The top panel displays  $\Delta(RF)$ , the mean error of the RF power, where the mean is over two quantities, the channels in the RF spectrum and the 256 trials.  $\Delta(RF)$  represents an offset bias in the derived RF powers. The units are Kelvins and the mean system temperature is 32.5 K, so an error of 0.1 K is a fractional error of 0.3%.
2. The bottom panel displays  $\sigma(IF)$ , the RMS uncertainty of the IF gain spectrum, in units of the theoretical RMS. To calculate this, we first form the difference between (a) the mean IF gain spectrum averaged over the 256 trials and (b) the input, noise-free

IF gain spectrum. We consider only the central 200 channels and fit a second-order polynomial to eliminate broad baseline wiggles, which are more serious for smaller values of the fractional LO coverage  $h$ . With our 256 trials the number of independent measurements for each channel is  $256N$  and, with our 2 K input noise and 32.5 K system temperature, the ideal theoretical RMS is  $\frac{2/32.5}{\sqrt{256N}}$ .

For completeness, we could also present the RMS uncertainty of the RF power. However, those results are comparable to those of the IF gain, so we refrain from presenting these to save space.

Both  $\Delta(RF)$  and  $\sigma(IF)$  decrease with  $N$ , and some schemas are better than others. In particular, the MRN, MRN<sup>2</sup>, MRN<sup>1.7</sup>, and  $3^{\Delta N}$  schemas are all quite good.

## 8.2. Results: Relative Fourier Amplitudes, a Third Quality Indicator

The above two quality indicators do not tell the whole story, for two reasons. One, they are derived after baseline subtraction, which removes large-scale ripples in the frequency spectra; we expect such ripples to be larger when  $h$ , and thus  $N$ , is small. Two, schemas other than the minimum-redundancy one do not uniformly sample Fourier components, and so their Fourier amplitude spectra should be less uniform. Here the focus is on the *relative* Fourier amplitudes, so we define all amplitude spectra *F-Ampl* to be the actual amplitude divided by the minimum amplitude Fourier component for that spectrum.

Figure 5 displays Fourier amplitudes of the IF gain residual spectra for a selection of our schemas. The left-hand panel emphasizes the higher frequencies. The bottom three plots are for MR5,1, MR7,1, and MR11,1. With the uniform sampling in  $\Delta i_{nn'}$ , these provide quite uniform Fourier amplitudes at high frequencies; and as  $N$  increases from 5 to 11, the fractional LO coverage  $h$  increases, which decreases the amplitude of lower-frequency Fourier components. For MR7,2 and MR7,4, we have strong Fourier components at frequencies 256 and 128 cycles, respectively, over the 512-channel IF band. These Fourier components are easily understood, because they correspond to periods of 2 and 4 channels, respectively. The other schemas do not have uniform sampling in  $\Delta i_{nn'}$ , and this is reflected in their Fourier amplitudes, which are not very uniform at high frequencies.

The right-hand panel emphasizes the low frequencies. Generally, the low-frequency amplitudes are smaller for large fractional LO coverage  $h$ . This is reflected in the MR7,1, MR7,2, and MR7,4 spectra, as well as the MR7,1 and MR11,1 spectra. Also the other schemas emphasize larger  $h$  at the expense of uniform coverage in  $\Delta i_{nn'}$ , and this is reflected in their smaller low-frequency amplitudes.

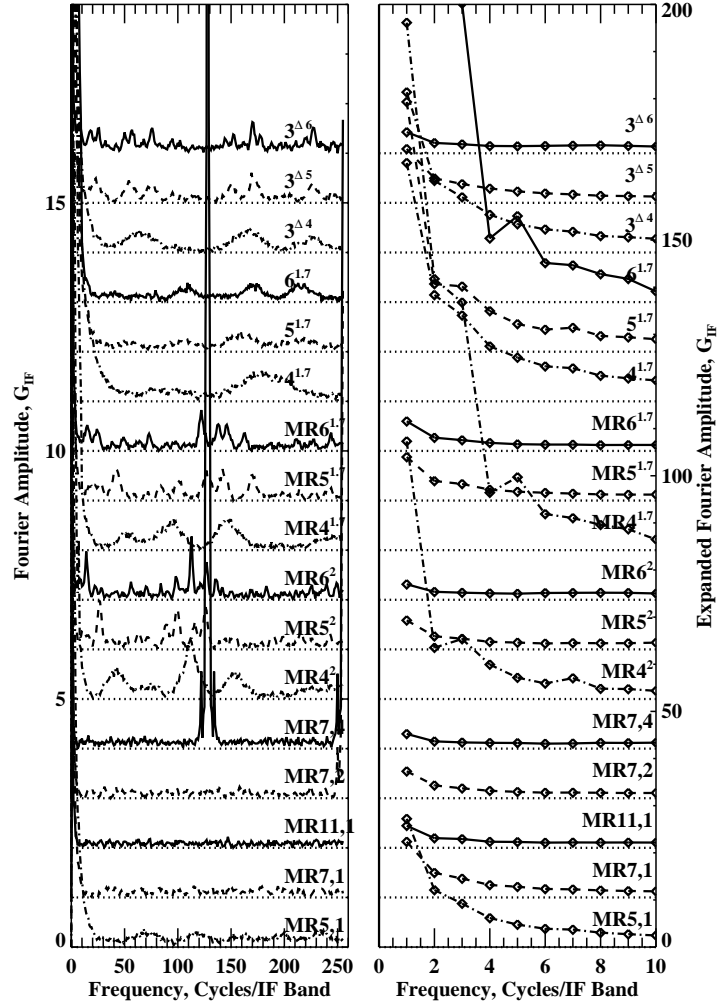


Fig. 5.— Plots of Fourier amplitude spectra of the IF gain residual spectra. The left panel exhibits the full frequency range from 1 cycle to 256 cycles per 512-channel IF band, with successive spectra displaced vertically by 1 unit. The right panel displays the low-frequency components by exhibiting the first 10 components (excluding the zero frequency component), with successive spectra displaced by 10.625 units.

The first Fourier coefficient serves as a proxy for the low-frequency Fourier components. Figure 6 plots the first Fourier amplitude  $F\text{-}Ampl[1]$  versus the fractional LO coverage  $h$ . As we anticipated,  $F\text{-}Ampl[1]$  decreases with  $h$ ; the dashed line is a minimum-absolute-residual-sum fit to the points, which fit de-emphasizes large deviations from the fit. The fit is

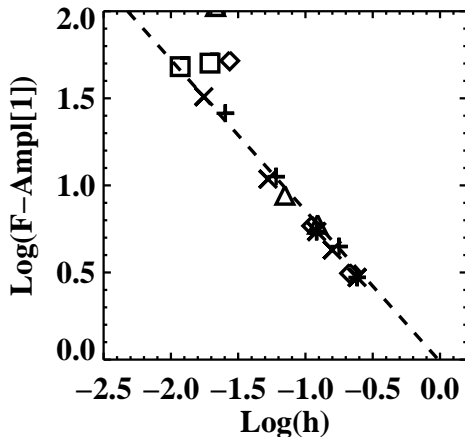


Fig. 6.— The amplitude of the first Fourier coefficient versus  $h$ , the fractional LO coverage. The dashed line is minimum-absolute-residual-sum fit to the points.

$$F-Ampl[1] \approx h^{-0.87} . \tag{32}$$

This parameter,  $F-Ampl[1]$ , is our third quality indicator, and we list it in column 4 of Table 1. For all reasonable schemas it is closely approximated by equation 32.

### 8.3. Summary: Which LSFS Schemas Are Best?

Which LSFS schema is best? If one wants the best accuracy and large  $N$  is not a problem, then the Minimum Redundancy (MRN) schema is ideal because it provides a flat, featureless spectrum of high-frequency Fourier amplitudes in Figure 5. If one is willing to sacrifice accuracy in favor of a smaller number of LO settings  $N$ , then one can consider the  $MRN^2$ ,  $MRN^{1.7}$ , and  $3^{\Delta N}$  schemas. These provide comparable results for  $N = 5$  and  $N = 6$ , with  $MRN^2$  having the edge. As a compromise between practicality and good results, our numerical experiments suggest the  $MRN^2$  schema, with  $N \geq 4$ .

## 9. SCHEMAS THAT HAVE $\min(\Delta i_{nn'}) > 1$

It is not strictly necessary for  $\min(\Delta i_{nn'})$  to equal unity; rather, it can equal some integer multiple, which we call  $R$ . Increasing  $R$  provides increased fractional LO coverage

$h$ , which may be desirable. We envision two circumstances where  $R > 1$  might be desirable. One is when spectral resolution can be degraded and one can bin the data into groups of  $R$  channels (§9.1). The other is when the number of spectral channels  $I$  is large: matrix sizes scale with  $I$  and the computational load for inverting a matrix scales with the cube of the matrix size, so using LSFS with large  $I$  and  $R = 1$  can be a problem. We can reduce this problem by using  $R^{th}$  sampling (§9.2).

### 9.1. Binning

If one wants to derive the IF gain spectrum and has prior knowledge that it varies slowly with frequency, then one can increase the fractional LO coverage  $h$  by increasing  $R$  and, also, bin the data into  $R$  channels and sacrifice resolution. Mathematically, this combination is identical to a dataset with  $R = 1$ .

### 9.2. $R^{th}$ Sampling

This technique retains full spectral resolution while keeping the matrix sizes manageable by using the following subterfuge. Suppose  $I = 4096$ . Convert the 4096-long spectrum into a series of  $R$  subspectra, each of length  $\frac{4096}{R}$ , by choosing every  $R^{th}$  point. For example, for  $R = 8$ , one creates 8 subspectra, each 512 channels long, each spanning nearly the full frequency range covered by the original 4096 channels. One uses LSFS on the  $R$  subspectra independently and patches the  $R$  result spectra together. For each subspectrum, the smallest LO spacing is equal to the bin separation, so each solution is mathematically identical to that for 512 channels and  $R = 1$ .

We did our numerical experiment for two schemes, the MR5,8-x scheme and the MR5<sup>2</sup>,8-x scheme; here the suffix “-x” signifies this  $R^{th}$  sampling scheme. Table 1 lists the quality indicators for these two experiments; they are comparable to the  $R = 1$  versions, which is reasonable because the mathematical equivalence of the  $R$  solutions.

The method is not perfect. Figure 7 shows the Fourier amplitude spectrum of the 4096-channel IF gain spectrum. The bottom panels show the full range of frequencies, 1 to 2048 cycles over the 4096-channel IF band. The most striking thing about these spectra are the spikes, which lie at multiples of 512 cycles per IF band. This is easily understood, because the band contains 4096 channels; 512 cycles per IF band corresponds to a period of 8 channels, which is the value of  $R$ . This shows that each of the  $R$  subspectra is slightly offset in power from the others, which is a result of their being reduced independently. Next,

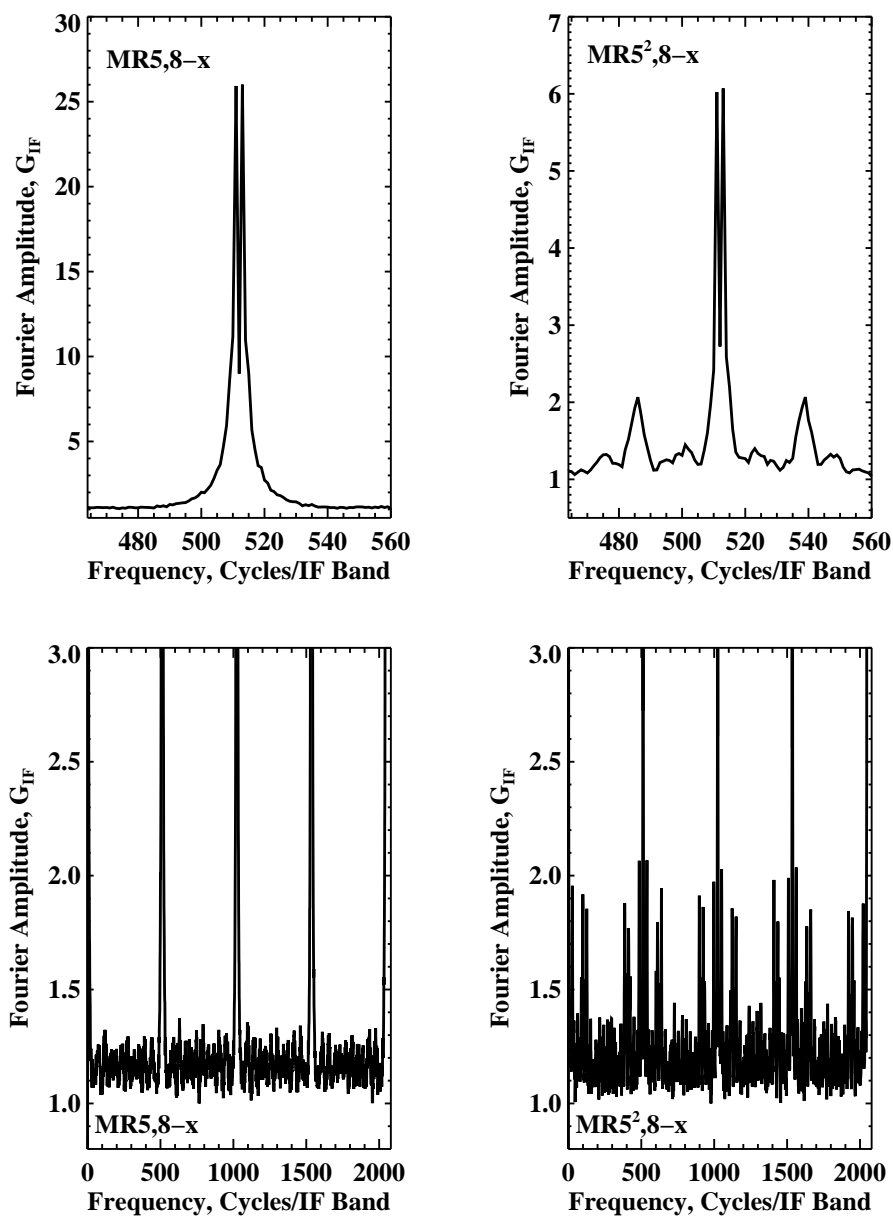


Fig. 7.— Numerical experimental Fourier amplitude spectra of the IF gain spectra for the two schemes MR5,8-x (left panels) and MR5<sup>2</sup>,8-x (right panels). The bottom panels show the full frequency range and cut off the peaks; the top panels show a magnified frequency range centered at 512 cycles per IF band. Note the difference in vertical scale for the top panels! The peaks repeat almost identically at multiples of 512.

spikes repeat, almost identically, at multiples of 512. This repetition can be understood in terms of the Fourier convolution theorem: the original data are, in effect, multiplied by a function that repeats every  $R$  channels; in the transform domain, the spectrum is convolved by the Fourier transform of this function, which produces the repetition.

The left-hand panels of Figure 7 show MRN,R-x and the right MRN<sup>2</sup>,R-x. The top panels show expanded views around 512 cycles per IF band. Note the difference in scale for the top panels: the MRN,R-x schema has much bigger Fourier peaks at the 512-cycle multiples and much smaller and more uniform Fourier amplitudes in between. In contrast, the MRN<sup>2</sup>,R-x has about four times smaller peaks, but stronger and less uniform Fourier amplitudes in between.

One could reduce these Fourier spikes and gain accuracy in the derived results by associating an additive constant for each of the  $R$  result spectra and devising a minimization procedure to determine the values of the  $R$  constants. More appealing is using the conventional, well-known technique of Wiener filtering to eliminate the spikes. Wiener filtering would work especially well for the MRN,R-x result because the Fourier power is so concentrated.

### 9.3. No Binning: the MR7,R Schemas

Suppose that one observes with  $R \neq 1$  but does *neither* of the above tricks—neither binning nor  $R^{\text{th}}$  sampling. How do the solutions fare under these conditions? We performed numerical experiments for  $R = [2, 4, 8, 16]$  only for the MR7 scheme, and we denote these LO setting arrangements by the name MR7,R. We present the three quality indicators in Table 1 and show the derived IF gain spectra in Figure 8. As expected, larger  $R$  leads to smaller  $F\text{-Ampl}[1]$ , but the other two quality indicators are degraded.  $R \geq 8$  breaks down and is worthless.

Figure 8 exhibits IF gain difference spectra for  $R = [1, 2, 4, 8]$ , plotted against the background of the IF gain itself. The results for  $R = 1$  and 2 look reasonable. The result for  $R = 4$  looks reasonable except for the systematic periodic signal in the difference spectrum. This has a period of exactly 4 channels, which is the minimum LO spacing, and confirms our hunch that one cannot accurately reconstruct the input signals with Fourier components smaller than the minimum LO spacing. Of course, The Fourier amplitude spectra in Figure 5 show this behavior quantitatively, and shows also that for  $R = 2$  there is also a systematic periodicity of 2 channels. For  $R = 8$  the solution breaks down and becomes worthless; moreover, for 16 of the 256 trials the iterative solution discussed in §3.1 didn't converge. For

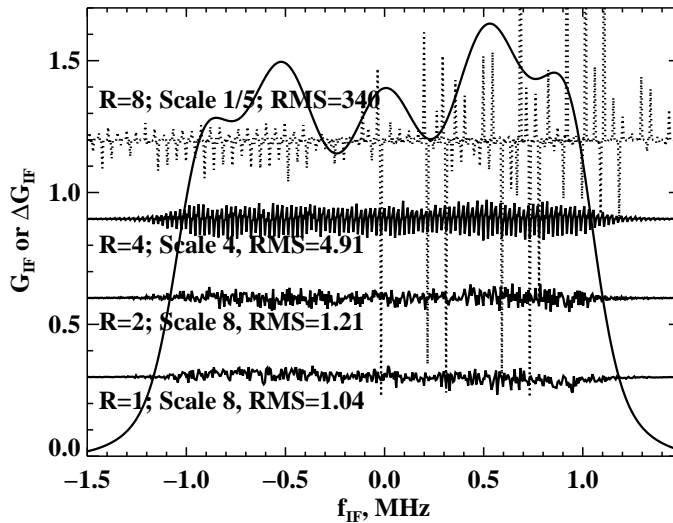


Fig. 8.— The noisy lines are the IF-gain difference spectra for  $R = [1, 2, 4, 8]$  versus  $f_{IF}$  for the MR7,R schema discussed in §9.3, scaled by the factors shown. The solid smooth line is the IF gain  $G_{IF}$  itself.

$R = 16$  the solutions never converged.

These results show that, with  $R > 1$ , one should use either the binning or the  $R^{th}$  sampling trick.

## 10. POLARIZED STOKES PARAMETERS: SWITCHING AND LSFS

Our above discussion applies to a single polarization, or to Stokes  $I$ . Here we generalize to the three polarized Stokes parameters ( $Q, U, V$ ). For discussion purposes, we discuss the example of native orthogonal linear polarizations, which produce time-variable voltages  $X$  and  $Y$ . We form Stokes parameters by taking time averages of the four possible products, whose results we denote by, for example,  $XX$ . The four Stokes parameters include the sum ( $XX + YY$ ), the difference ( $XX - YY$ ), the product  $2XY$ , and the product with  $90^\circ$  phase lag  $2YX$ ; for native linear polarizations, these combinations produce Stokes  $I, Q, U,$  and  $V$ , respectively. (For native circular polarizations, these combinations would produce Stokes  $I, V, U,$  and  $Q$ , respectively.) Part of the process of calibrating the Stokes parameters involves applying the Mueller matrix calibrations to these combinations as discussed by Heiles et al. (2001), and we assume these corrections have applied to these time-average products before



applying the discussion below, which covers how to obtain Stokes spectra from switching or the LSFS technique.

### 10.1. Position and Frequency Switching

Generating  $I$  and  $Q$  requires taking the sums and differences. For position and frequency switching, this is simply a matter of arithmetically combining the results in equations 5 and 7, respectively.

Generating  $U$  and  $V$  requires crosscorrelating the polarizations. Consider  $U$ , which we obtain from  $2XY$ . We write the counterpart of equation 3 as

$$P_U(f_{IF}) = [G_{XX,IF}(f_{IF}) G_{XX,RF}(f_{RF})]^{1/2} [G_{YY,IF}(f_{IF}) G_{YY,RF}(f_{RF})]^{1/2} \quad (33)$$

$$[(U_A(f_{RF}) + U_A) + (U_R(f_{RF}) + U_R)] .$$

Here the square-root of the gain products  $G$  appear because  $U$  is derived by multiplying voltages  $X$  and  $Y$ , while the gains  $G_{XX}$  and  $G_{YY}$  are power gains. We could write the equivalent of equations 5 and 7, but these would be algebraically cumbersome and would not convey much information. Usually, astronomical polarized signals are weak, so if we keep only zeroth order terms then the position- and frequency-switched spectra are simplified equivalents of equations 5 and 7, and they both become

$$\frac{P_U(f_{IF}) - P'_U(f_{IF})}{[P'_{XX}(f_{IF})P'_{YY}(f_{IF})]^{1/2}} \approx [U_A(f_{RF}) + (U_A - U'_A)] . \quad (34)$$

### 10.2. LSFS

LSFS also applies to polarized Stokes parameters obtained from crosscorrelation. The application of the LSFS procedure to  $XX$  and  $YY$  individually provides their associated RF powers and, more importantly for now, the IF gains  $G_{XX,IF}(f_{IF})$  and  $G_{YY,IF}(f_{IF})$ . Thus, in equation 33, we can treat them as known quantities and move them to the left-hand side, which is the same as pre-correcting the data for the IF gains.

With this, it is straightforward to duplicate the steps leading to equation 13. We begin with the analog of equation 8,

$$S_U(f_{RF}) = [G_{XX,RF}(f_{RF}) G_{YY,RF}(f_{RF})]^{1/2} [(U_A(f_{RF}) + U_A) + (U_R(f_{RF}) + U_R)] , \quad (35)$$

and carrying through the algebra we arrive at the equivalent of equation 13,

$$\frac{P_{U,i,\Delta i_n}}{G_{IF,i}} = S_{U,i+\Delta i_n}, \quad (36)$$

where to reduce clutter we write  $G_{IF,i} = [G_{XX,IF,i} G_{YY,IF,i}]^{1/2}$ .

The left-hand side contains the measured quantities and the right the desired unknown ones. In contrast to equation 13, there is only a single unknown on the right-hand side. This means that the least-squares solution for the unknowns is just the appropriate average of the left-hand quantities. Alternatively, we can follow the line of development pursued in §3 and express the solution as a least-squares problem using matrices. This is more time-consuming computationally, but much simpler programmatically and offers more flexibility. In contrast to the the situation in §3, this least-squares fit is a linear one so it is not necessary to do an iterative solution. Neither do we need to add the additional constraint embodied in equation 19.

Referring to §3.2, here the number of measurements is  $M = NI$  ( $I$  channels for each of the  $N$  LO frequencies) and because we do not have to determine the gains ( $\delta G_i$ ) the number of unknowns is only  $a = (I + \Delta i_{N-1})$ . To make the number of measurements exceed the number of unknowns, we require  $N > (1 + h)$ , which is more easily satisfied than the corresponding equation 22. The current  $\mathbf{X}$  matrix has  $NI$  rows and  $(I + \Delta i_{N-1})$  columns. For our textbook example of §3.3, the correspondent to equation 26 looks like

$$\mathbf{X} = \begin{bmatrix} 1 & 0 & 0 & 0 & 0 & 0 & 0 \\ 0 & 1 & 0 & 0 & 0 & 0 & 0 \\ 0 & 0 & 1 & 0 & 0 & 0 & 0 \\ 0 & 0 & 0 & 1 & 0 & 0 & 0 \\ 0 & 1 & 0 & 0 & 0 & 0 & 0 \\ 0 & 0 & 1 & 0 & 0 & 0 & 0 \\ 0 & 0 & 0 & 1 & 0 & 0 & 0 \\ 0 & 0 & 0 & 0 & 1 & 0 & 0 \\ 0 & 0 & 0 & 1 & 0 & 0 & 0 \\ 0 & 0 & 0 & 0 & 1 & 0 & 0 \\ 0 & 0 & 0 & 0 & 0 & 1 & 0 \\ 0 & 0 & 0 & 0 & 0 & 0 & 1 \end{bmatrix}. \quad (37)$$

In this matrix, the arrangement of rows and columns is similar to that in equation 26, except that the IF gains do not appear. Here in equation 37, we have

1. The first four rows pertain to the lowest LO frequency with  $\Delta i_0 = 0$
2. The next two pairs of four rows pertain to  $\Delta i_1 = 1$  and  $\Delta i_2 = 3$ .
3. The last seven columns are the coefficients of the seven RF powers  $\delta s_{i+\Delta i_n}$  in equation 18.

## 11. LSFs versus Switching

The traditional technique for heterodyne spectroscopy is called “switching”. It involves taking an off-source reference spectrum. This technique has been used by radioastronomers for decades. We offer a few comments that compare the two techniques. These comments are based mainly on our observing experience over the years and the numerical simulations discussed above. Unfortunately, we have not experimentally investigated these matters with LSFs spectra because our observing experience with this technique is limited to a handful of projects.

### 11.1. Channel-to-channel noise

First, consider  $\sigma(IF)$ , the channel-to-channel noise for the IF gain. Figure 4 displays  $\sigma(IF)$  for various LSFs schemas. These dispersions are normalized to the ideal, for which the noise is determined by the time-bandwidth product—where the time is the *full* integration time used for all LO settings. A value of unity would result if the LSFs fit provided no degradation in noise. All the values shown on Figure 4 are less than 2.

It is important to recall the noise in a conventional position- or frequency-switched spectrum. Conventionally, for a switched spectrum half the total observing time is spent on the OFF spectrum; this reduces the sensitivity of the ON spectrum by  $\sqrt{2}$ . Subtracting the equally noisy OFF spectrum reduces the sensitivity by another factor  $\sqrt{2}$ . Thus, a conventional switched spectrum has  $\sigma(IF) = 2$ . All of the points displayed on Figure 4 have better sensitivity than a conventional switched spectrum!

### 11.2. Baseline wiggles

Next, consider the slow undulations of the RF power spectrum with frequency, commonly referred to as “baseline wiggles”. For conventional switched spectra, our discussion

of §2 shows that the baseline wiggles are determined by the frequency dependence of the RF power, which is in turn determined by reflections, the RF gain, and system temperature. These are instrumental properties associated with the telescope structure, RF amplifiers, and associated circuitry; they change slowly with time. Thus they do not tend to decrease with increased integration time.

For LSFS spectra, there are two sources of baseline wiggles. One is these *intrinsic* wiggles that reside in the RF power spectrum. These often occur from reflections, as explained in §1. LSFS will not eliminate these. On the contrary, it is very useful for determining them, just as we did in our detailed discussion of reflection-induced baseline wiggles at Arecibo<sup>2</sup>. We emphasize that these intrinsic wiggles are not artifacts introduced by LSFS because they are actually present in the RF power spectrum that enters the feed. LSFS will determine these intrinsic wiggles but, in contrast to frequency-switched spectra, it will not exacerbate them.

The other type of baseline wiggle in LSFS spectra is associated with the *fitting* of low-frequency Fourier amplitudes shown in the right-hand panel of Figure 5. The nonflat Fourier amplitudes reveal that some Fourier components are reproduced less accurately than others. In particular, the amplitudes increase for larger wavelengths, i.e., for slower variations with frequency—leading to baseline wiggles.

This fitting type of LSFS wiggle should decrease with increased integration time because there should be no systematic bias in the *phase* of the fitted LSFS Fourier components. Rather, the amplitudes are less well determined, leading to increased noise, but the location of a positive-going fitted baseline ripple should change from one integration to the next.

## 12. SUMMARY

We described a new technique for obtaining accurate results from heterodyne spectroscopy. It involves taking measurements at 3 or more local oscillator (LO) frequencies and using least squares to derive the RF power and IF gain spectra as individual entities. We call this the Least-Squares Frequency-Switching (LSFS) technique. We have used the technique in two ways: one, to obtain a single IF gain spectrum used to correct a series of several thousand mapping measurements; and two, to obtain the RF power spectrum directly during a long integration.

---

<sup>2</sup>See Heiles, Carl 2005, “Some Characteristics of ALFA’s Fixed Pattern Noise (FPN)”, Arecibo Technical memo 2005-04, available at [http://www.naic.edu/science/techmemos\\_set.htm](http://www.naic.edu/science/techmemos_set.htm)

We discussed mathematical details and computational requirements of the technique and explored optimum observing schemas using numerical experiments. The quality of the results depends on the choice of the LO frequencies, and §8.3 summarizes our results and recommendations.

We illustrate the method with three real-life examples. In one of practical interest (§4), we created a large contiguous bandwidth aligning three smaller bandwidths end-to-end; radio astronomers are often faced with the need for a larger contiguous bandwidth than is provided with the available correlator. In §9 we outlined an approach suitable for computationally difficult cases as the number of spectral channels grows beyond several thousand.

This work was supported in part by NSF grant AST-0406987 and, also, by the NAIC. Josh Goldston Peek and Snezana Stanimirović read an early version of the manuscript and made several important suggestions, and Benjamin Winkel made several valuable comments on a later draft.

## REFERENCES

- Heiles, C., Perillat, P., Nolan, M., Lorimer, D., Bhat, R., Ghosh, T., Lewis, M., O’Neil, K., Salter, C., Stanimirović, S. 2001, *PASP*, 113, 1274
- Moffett, A. 1968, *IEEE Trans Ant Prop AP-16*, 72
- Ishiguro, M. 1980, *Radio Science*, 15, 1163
- Press, W.H., Teukolsky, S.A., Vetterling, W.T., & Flannery, B.P. 1992, *Numerical Recipes in C*, Second Edition, section 15.4
- Stanimirović, S., Putman, M., Heiles, C., Peek, J. E. G., Goldsmith, P. F., Koo, B.-C., Kreo, M., Lee, J.-J., Mock, J., Muller, E., Pandian, J. D., Parsons, A., Tang, Y., Werthimer, D. 2006, *ApJ*, 653, 1210